Hindawi Publishing Corporation
Journal of Theoretical Chemistry
Volume 2016, Article ID 7909576, 19 pages
http://dx.doi.org/10.1155/2016/7909576

Research Article

Concomitant Effects of Transition Metal Chelation and Solvent Polarity on the First Molecular Hyperpolarizability of 4-Methoxyacetophenone Thiosemicarbazone: A DFT Study

Nyiang Kennet Nkungli and Julius Numbonui Ghogomu

Laboratory of Noxious Chemistry and Environmental Engineering, Department of Chemistry, Faculty of Science, University of Dschang, P.O. Box 67, Dschang, Cameroon

Correspondence should be addressed to Julius Numbonui Ghogomu; ghogsjuju@hotmail.com

Received 2 July 2016; Accepted 4 October 2016

Academic Editor: Anton Kokalj

Nonlinear optical (NLO) properties of organic and metal-organic materials are of considerable interest to emerging optoelectronic and photonic technologies. Much work has been carried out on the former materials but the latter ones have received less attention till date. Herein, a density functional theory (DFT) study on the combined effects of transition metal chelation and solvent polarity on the first hyperpolarizability (β_{tot}) of 4-methoxyacetophenone thiosemicarbazone (MAPTSC) is reported. MAPTSC exhibits a tautomeric form with higher optical nonlinearity rendering its NLO response in polar solvents potentially switchable. Our results have revealed significant modifications of the first hyperpolarizability of MAPTSC upon complexation with different transition metal chlorides in the presence of solvents with varying dielectric constants. Therefore, its second-order NLO response is highly tunable by the synergy of transition metal chelation and solvent polarity. MAPTSC and its Zn(II) and Pt(II) chloride complexes are promising NLO materials because their gas-phase β_{tot} values are larger than those of the prototype push-pull molecules, *para*-nitroaniline (PNA) and urea, by factors of about 1.40–1.76 and 19.57–37.24, respectively; these factors greatly increase in polar solvent medium. Moreover, they possess high optical transparencies in the visible region of the electromagnetic spectrum which mitigate transparency/nonlinearity trade-offs, thereby increasing the likelihood of broad band NLO response.

1. Introduction

Nonlinear optical (NLO) materials have recently received considerable attention because of their potential applications in the optoelectronic and all-optical (photonic) devices of telecommunication, optical switching, optical signal processing, optical transmission, optical data storage, optical computing, and so forth, [1, 2]. They are also essential for photodynamic therapy, biological imaging, and the protection of human eyes and optical sensors (by NLO materials with optical limiting effects) from high intensity LASER beams [3, 4]. NLO effects arise from the interaction of an applied optical field (usually LASER) with the electronic field created by the oscillation of electrons in a NLO material, generating a new optical field that is altered in frequency, amplitude, phase, or any other physical property [5–7]. Very high light intensities typically provided by LASERS are required for optical nonlinearity to be observed [8]. NLO effects include saturable absorption (SA), reverse saturable absorption (RSA), second-harmonic generation (SHG), two-photon absorption (TPA), and optical limiting [8, 9].

Recently, the first hyperpolarizability (β_{tot}) has been under rigorous investigation because a large β_{tot} value is a prerequisite for large and fast second-order or quadratic NLO response. Other necessary conditions for significant quadratic NLO properties in molecular materials include noncentrosymmetry, low optical loss, high thermal and mechanical stability, intense low-energy electronic transitions with charge transfer (CT) character, and significant intramolecular charge transfer (ICT) owing to electron cloud movement from an electron donor to an electron acceptor through a π-conjugate bridge [10, 11]. Molecules with

excellent NLO properties usually contain an electron-donor group (D) and an electron-acceptor group (A) linked through an intervening π-conjugated framework, forming the so-called D-π-A structure or push-pull system [12, 13]. Effective methods of enhancing the second-order NLO responses of materials involve increasing the donor-acceptor capabilities of D and A and increasing the length of the π-conjugated pathway between them [2, 9, 14].

Important candidates in the area of NLO chromophores are organic and metal-organic materials. For the latter, transition metal complexes with π-conjugated ligands are interesting for the construction of multifunctional NLO chromophores by virtue of their rich photochemical and photophysical properties, greater design flexibility, excellent chemical stability, and intense low-energy metal-to-ligand charge transfer (MLCT), as well as ligand-to-metal charge transfer (LMCT) electronic transitions [2, 15]. From literature survey, the vast majority of molecules investigated for NLO effects are purely organic push-pull systems. Comparatively, transition metal complexes containing π-conjugated organics are less explored in this area despite their potentials of combining the high optical nonlinearity and chemical flexibility of organic materials with the physical ruggedness of inorganic materials. In an effort to bridge this gap, the impact of metal complexation on the NLO responses of purely organic push-pull systems is currently being investigated. In this perspective, we chose 4-methoxyacetophenone thiosemicarbazone (MAPTSC) as our organic push-pull system because thiosemicarbazones and their metal complexes are notable materials for SHG and, as such, are highly applicable in the field of nonlinear optics [16]. The extensive electron delocalization in the thiosemicarbazone (TSC) moiety greatly improves the SHG efficiency of free TSC ligands and their metal complexes [17]. Furthermore, acetophenone thiosemicarbazone (APTSC) has been identified by means of the Z-scan technique as a NLO material with third-order harmonic generation capability [17]. Because MAPTSC has a powerful electron donor ($-OCH_3$) appended to the benzene ring which is not the case in APTSC. The NLO response of the former is expected to be larger and faster than that of the latter. Moreover, MAPTSC like many TSCs readily forms chelates with transition metals. Several of its transition metal complexes, including most of those currently studied, have been successfully synthesized, crystallized, and characterized [18].

Herein, we report for the first time on the combined effects of transition metal coordination by MAPTSC and solvent polarity and on its first molecular hyperpolarizability. Specifically, the β_{tot} values of MAPTSC and its Ni(II), Pd(II), Pt(II), Cu(II), and Zn(II) chloride complexes in vacuo and in solvents with different dielectric constants have been calculated and compared. In an attempt to explain the modifications undergone by the β_{tot} value of MAPTSC following its complexation with different transition metal ions and due to changes in solvent polarity, the relationship between β_{tot} values of all molecules studied and their frontier molecular orbital (HOMO-LUMO) energy gaps has been sought. In the same vein, the relationship between these β_{tot} values and photoinduced electronic transitions in the molecules has been investigated. Time-dependent density functional theory (TD-DFT) calculations, natural bond orbital (NBO) analysis, and charge decomposition analysis (CDA) have been carried out in order to determine the charge transfer (CT) capabilities, optical transparencies in the visible region of the electromagnetic (EM) spectrum, electron delocalization, and orbital interaction patterns of the molecules. Owing to the complications encountered during the experimental measurement of NLO activities of materials by the Z-scan technique, quantum chemical calculations remain a fascinating alternative. For this study, the density functional theory (DFT) was preferred over *ab* initio methods because DFT calculations, with pseudopotentials, are the standard approach for computations on transition metal containing systems [19]. Moreover, the DFT is very instrumental in designing molecules for NLO applications [14] because of its remarkable accuracy/computational-time ratio, coupled with the fact that it takes good account of electron correlation effects in calculations.

2. Computational Details and Background Theory on Second-Order NLO Response

All theoretical calculations were carried out with the Gaussian 09W suite of programs [20]. The molecular geometries of MAPTSC and its Ni(II), Pd(II), Pt(II), Cu(II), and Zn(II) chloride complexes were optimized without constraints of any kind in gas and solvent phases using Becke's three-parameter Lee-Yang-Parr hybrid functional [21] in conjunction with the small core Stuttgart-Dresden pseudopotential (SDD) for the transition metals, and the Pople-style basis set 6-31++G(d,p) for every other element. Then, harmonic vibrational frequencies were computed at the same level of theory as that used for geometry optimization to ascertain that each of the optimized geometries is a local minimum on its potential energy surface. For all calculations reported herein, the restricted closed-shell Kohn-Sham model was adopted for the closed-shell molecules (MAPTSC and its Ni(II), Pd(II), Pt(II), and Zn(II) chloride complexes), whereas the unrestricted Kohn-Sham model was used for the open-shell Cu(II) chloride complex.

Bulk solvent effects were taken into account by the integral equation formalism polarizable continuum model (IEF-PCM). Three types of solvents, namely, benzene (a nonpolar solvent), ethanol (a polar protic solvent), and dimethyl sulfoxide, DMSO (a polar aprotic solvent), were used for investigation of solvent effects on the first hyperpolarizabilities of the molecules studied. For all compounds investigated, first hyperpolarizability (β_{tot}) values were calculated at the B3LYP/6-31++G(d,p)/(SDD for metal ions) and B3LYP/6-311++G(d,p)/(SDD for metal ions) levels of theory, for comparison. Vertical excitation energies to the first 10 singlet excited states were computed using TD-DFT method at CAM-B3LYP/6-31++G(d,p)/(SDD for metal ions) level of theory. The corrected asymptotic behavior of the CAM-B3LYP (Coulomb-attenuating method applied to B3LYP) functional improves accuracy especially in the higher regions of the electronic spectrum. Natural transition orbital (NTO) analyses were performed in order to describe the

singlet "particle-hole" pairs involved in the dominant electronic transitions in all molecules studied. Natural transition orbitals (NTOs) provide a better qualitative description of electronic excitations. They are obtained by transforming the canonical molecular orbitals into a more compact form in which each excited state is most often represented by a single pair of orbitals, the "particle" and the "hole." An electronic excitation from "particle" to "hole" is weighted with an eigenvalue [22].

The first molecular hyperpolarizabilities of MAPTSC and its complexes were calculated by the finite field method as implemented in Gaussian 09W. In a static electric field F, the energy of an isolated molecule can be written as a Taylor series expansion with respect to the electric field, as shown in the following equation [5, 23]:

$$E = E_0 - \mu_i F_i - \frac{1}{2}\alpha_{ij}F_iF_j - \frac{1}{6}\beta_{ijk}F_iF_jF_k - \frac{1}{24}\gamma_{ijkl}F_iF_jF_kF_l - \cdots. \quad (1)$$

In this equation, E_0 is the energy of the unperturbed molecule (the molecular energy without the applied electric field), F_i is the field at the origin, μ_i is the permanent dipole moment vector, and α_{ij}, β_{ijk}, and γ_{ijkl} are the polarizability, first static hyperpolarizability, and second static hyperpolarizability tensors, respectively. The subscripts i, j, and k label the x, y, and z components, since the external electric field is applied to the molecule with coordinates along x, y, and z directions [13, 24]. The first static hyperpolarizability tensor β_{tot} is defined as

$$\beta_{\text{tot}} = \left(\beta_x^2 + \beta_y^2 + \beta_z^2\right)^{1/2}, \quad (2)$$

where β_x, β_y, and β_z are the components of β_{tot} along the x, y, and z axes, respectively [23, 25, 26]. From the components of the β_{tot} tensor, the values of β_x, β_y, and β_z are calculated as follows:

$$\begin{aligned}\beta_x &= \left(\beta_{xxx} + \beta_{xyy} + \beta_{xzz}\right);\\ \beta_y &= \left(\beta_{yyy} + \beta_{yzz} + \beta_{yxx}\right);\\ \beta_z &= \left(\beta_{zzz} + \beta_{zxx} + \beta_{zyy}\right).\end{aligned} \quad (3)$$

Therefore, the complete equation used to calculate the magnitude of β_{tot} is

$$\beta_{\text{tot}} = \left[\left(\beta_{xxx} + \beta_{xyy} + \beta_{xzz}\right)^2 + \left(\beta_{yyy} + \beta_{yzz} + \beta_{yxx}\right)^2 + \left(\beta_{zzz} + \beta_{zxx} + \beta_{zyy}\right)^2\right]^{1/2}. \quad (4)$$

3. Results and Discussion

3.1. The Push-Pull Structures and Optimized Geometries of the Molecules Studied. MAPTSC undergoes rapid and facile thione-thiol tautomerization via the exchange of a proton between the hydrazinic nitrogen and the thionic sulfur of the thiosemicarbazone (TSC) moiety [16]. It can act as an N- and S-donor bidentate neutral ligand (thione tautomer) and as an anionic ligand (deprotonated thiol tautomer) [27]. Much attention in this paper has been focused on the thione tautomer of MAPTSC and its complexes because the thione tautomer is the predominant form of thiosemicarbazones [28]. The push-pull CT mechanisms of the thione tautomer (L1) and thiol tautomer (L2) of MAPTSC are depicted in Figures 1(a) and 1(b), respectively. In both tautomers, the electron donor (D) is the methoxy group ($-OCH_3$). The electron acceptor (A) in L1 and L2 is the hydrazinic N–H and the amino (NH_2) groups of the TSC moiety, respectively. As such, the π-conjugated pathway linking A and D in L1 is made up of the benzene ring and the appended azomethine group of the thionic TSC moiety, while that in L2 is comprised mainly of the benzene ring and the two attached conjugated azomethine groups of the thiolic TSC moiety. Hence, the π-conjugated bridge for the D-π-A structure is shorter in L1 than that in L2, and this can lead to the tautomers exhibiting different optical nonlinearities. Based on the length of the π-bridge between A and D, the NLO response of L2 should be stronger than that of L1. A large difference in the optical nonlinearities of the tautomers will render the NLO response of MAPTSC switchable, since L1 and L2 are both stable at room temperature and can be interchanged via thione-thiol tautomerization.

The scenario in the transition metal chloride complexes of MAPTSC is different from that in the free ligands, because L2 loses its thiolic hydrogen via deprotonation as it chelates metal ions. The loss of the thiolic hydrogen and the stability of the chelate ring hinder thione-thiol tautomerization of MAPTSC. As a result, a switchable NLO response based on thione-thiol tautomerism is least expected in the complexes. In this paper, the NLO properties of the Ni(II), Pd(II), Pt(II), Cu(II), and Zn(II) chloride complexes of L1 have been studied. To facilitate the presentation and comprehension of our results, the gas-phase optimized geometries of these molecules visualized using Gauss View 5.0.8 [29] are shown in Figure 2.

Charge decomposition analysis (CDA) was performed in order to determine the nature of the coordination bonds between L1 and the transition metal ions M(II) present in the metal chloride fragments (MCl_2). In addition, CDA was used to investigate the impact L1–MCl_2 binding may have on the D-π-A charge transfer mechanisms in the complexes. Furthermore, CDA was used to study the influence of any ambivalent donor-acceptor behavior of the transition metals on the push-pull CT capabilities of the complexes investigated. CDA was first proposed by Dapprich and Frenking [30] and has been generalized by Xiao and Lu [31] from its original formulation. Besides CDA, extended charge decomposition analysis (ECDA) proposed by Gorelsky and coworkers [32] was performed. These methods are capable of providing a deep insight into how electronic charge is transferred between L1 (fragment 1) and MCl_2 (fragment 2) in the complexes for charge equilibrium to be attained. Typically, CDA defines two components of intermolecular CT: forward donation (σ-bonding) and back donation or back-bonding (π-bonding). This has made CDA a popular method for

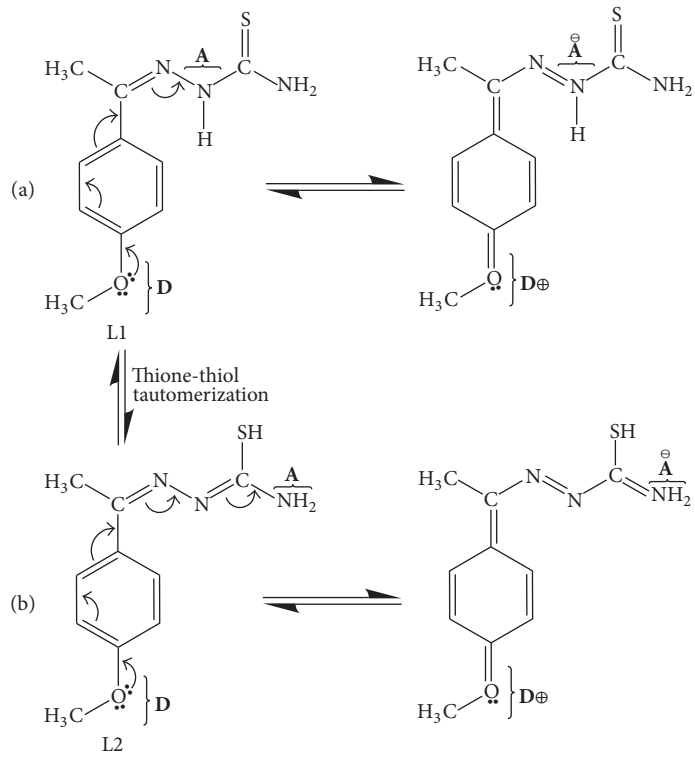

Figure 1: Schematic representation of the push-pull mechanisms of the thione and thiol tautomers of MAPTSC, where **A** is the electron-acceptor group and **D** is the electron-donor group.

estimating the amount of electron delocalization in donor-acceptor complexes [33] and in the donor-acceptor metal-ligand bonds in coordination complexes. The generalized CDA and ECDA were carried out using Multiwfn 3.3.8 [34] based on input files obtained from single-point calculations at B3LYP/6-311G(d,p)/(SDD for metal ions) level of theory. The results of CDA and ECDA on the molecules studied are presented in Table 1.

From the donation to back donation ratios, $|d/b|$ in Table 1, it is obvious that the coordination bonds in the Ni(II), Cu(II), and Zn(II) chloride complexes of L1 are predominantly sigma covalent bonds with very little π-character. The transition metal ions in these complexes act mainly as electron acceptors, since back donation is insignificant compared to donation. The electrons donated by L1 are mainly coming from filled π-bonding orbitals and/or the lone electron pair orbitals of its N- and S-donor atoms and are received in empty orbitals of the transition metal ions. The $|d/b|$ values for $[Pd(L1)Cl_2]$ and $[Pt(L1)Cl_2]$ clearly show that their coordination bonds have a substantial π-character, which helps to extend the π-conjugated pathway for the push-pull systems to the Pd(II) or Pt(II) ions in the respective complexes. The back donated electrons originate from filled d-orbitals of the transition metal ions and are received in empty π^*-antibonding orbitals on L1. The values of electron donation and back donation have shown that the Pd(II) and Pt(II) ions are capable of ambivalent electron donor-acceptor behaviors in their respective complexes studied in this research endeavor. Such ambivalent electron donor-acceptor capabilities can trigger redox processes that may lead to switchable NLO activities in the complexes. As clear from Table 1, back donation of electrons has witnessed a moderate to drastic increment in the bulk solvents, implying that the solvent environment (especially that created by the highly polar solvents) increases the π-character of the metal-ligand coordination bonds in the complexes investigated.

3.2. First Molecular Hyperpolarizabilities of MAPTSC and Its Complexes. The first molecular hyperpolarizabilities (β_{tot}) of MAPTSC and its complexes studied (listed in Table 2) were calculated using (2) based on the x, y, and z components (β_x, β_y, and β_z) of β_{tot}. The values of β_x, β_y, and β_z were computed from the components of the β_{tot} tensor: β_{xxx}, β_{yxx}, β_{xyy}, β_{yyy}, β_{zxx}, β_{xyz}, β_{zyy}, β_{xzz}, β_{yzz}, and β_{zzz}, using (3). The components of the β_{tot} tensor for each molecule studied were obtained via Gaussian 09W calculations at two levels of theory: B3LYP/6-31++G(d,p)/(SDD for metal ions) and B3LYP/6-311++G(d,p)/(SDD for metal ions) in gas and solvent phases. The trends adopted by the β_{tot} values on going from the gas to the solvent phase have been elucidated graphically in Figure 3. The β_{tot} values calculated using the data obtained from Gaussian calculations are usually in atomic units, but those reported in this paper have been converted into electrostatic units using the conversion factor 1 a.u. = 8.6393×10^{-33} esu. Inspection of the values in Table 2 and the graphs in Figure 3 has revealed similar trends adopted by the β_{tot} values of each molecule (calculated at both levels of theory) on passing from the gas to the solvent phase.

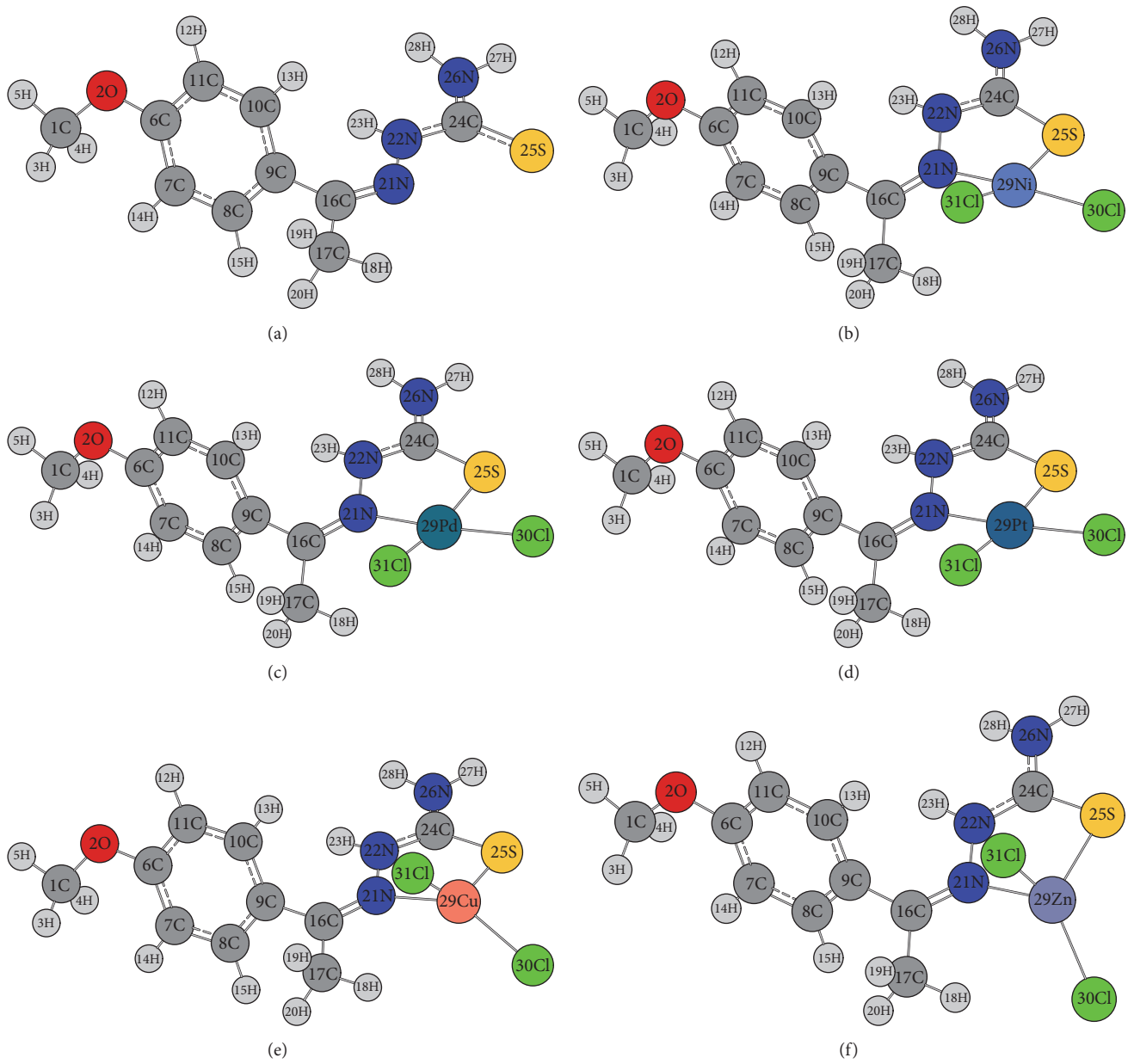

Figure 2: Optimized geometries of (a) ligand L1, (b) $[Ni(L1)Cl_2]$, (c) $[Pd(L1)Cl_2]$, (d) $[Pt(L1)Cl_2]$, (e) $[Cu(L1)Cl_2]$, and (f) $[Zn(L1)Cl_2]$ at B3LYP/6-31++G(d,p)/(SDD for metal ions) level of theory.

Except for a few cases, the β_{tot} values calculated at the former level of theory are larger than those calculated at the latter level. Hence, further discussion in this paper regarding the β_{tot} values and associated second-order NLO activities of the molecules is based only on the results obtained at the B3LYP/6-31++G(d,p)/(SDD for metal ions) level of theory.

The magnitude of the β_{tot} value for MAPTSC calculated in the present work is highly dependent on the tautomer present and on the nature of the surrounding environment. For instance, the β_{tot} value for L1 is 7.298×10^{-30} esu in gas-phase and 19.282×10^{-30} esu in DMSO, while that for L2 is 11.079×10^{-30} esu in gas-phase and 24.945×10^{-30} esu in DMSO. The gas-phase β_{tot} values of the thione-thiol tautomers of MAPTSC are approximately 0.92–1.40 times larger than that of *para*-nitroaniline (7.9×10^{-30} esu [35]), a prototype push-pull molecule [36], and about 19.57–29.71 times larger than that of urea (372.89×10^{-33} esu [37]), indicating that MAPTSC is a potent NLO material. From the β_{tot} values of the thione-thiol tautomers of MAPTSC, it is clear that the second-order NLO response of MAPTSC is potentially switchable especially in polar solvents, due to the presence of a tautomeric form (thiol form) with a higher CT capability. Since thione-thiol equilibrium is readily influenced by factors such as the nature of the solvent,

Table 1: ECDA and generalized CDA results for transition metal chloride complexes of L1 calculated using Gaussian output files for single-point calculations at B3LYP/6-311G(d,p)/(SDD for metal ions) level on geometries optimized at B3LYP/6-31++G(d,p)/(SDD for metal ions) level.

Complexes[a]	$[Ni(L1)Cl_2]$	$[Pd(L1)Cl_2]$	$[Pt(L1)Cl_2]$	[Cu(L1)Cl2][b]	$[Zn(L1)Cl_2]$
Gas-phase					
Frag.1 → Frag.2 donation (*d*)	0.26654	0.14418	0.21067	0.30532	0.26154
Frag.1 ← Frag.2 back donation (*b*)	−0.00296	0.04153	0.05289	−0.01265	0.00267
Net Frag.1 → Frag.2 donation (*d*-*b*)	0.26950	0.10266	0.15778	0.31797	0.25887
Donation to back donation ratio, |*d*/*b*|	89.95478	3.47205	3.98336	24.13581	98.02661
CT(1 → 2) - CT(2 → 1)	0.60450	0.39720	0.46260	0.56460	0.41070
Benzene					
Frag.1 → Frag.2 donation (*d*)	0.28205	0.15715	0.21982	0.33276	0.29419
Frag.1 ← Frag.2 back donation (*b*)	−0.00731	0.03463	0.04368	−0.01384	0.00387
Net Frag.1 → Frag.2 donation (*d*-*b*)	0.28936	0.12253	0.17615	0.34659	0.29032
Donation to back donation ratio, |*d*/*b*|	38.56248	4.53860	5.03318	24.05183	76.07706
CT(1 → 2) - CT(2 → 1)	0.69220	0.49480	0.55910	0.66880	0.46970
Ethanol					
Frag.1 → Frag.2 donation (*d*)	0.29623	0.16990	0.22919	0.35717	0.32350
Frag.1 ← Frag.2 back donation (*b*)	−0.00861	0.02929	0.03645	−0.01264	0.00671
Net Frag.1 → Frag.2 donation (*d*-*b*)	0.30484	0.14061	0.19274	0.36981	0.31679
Donation to back donation ratio, |*d*/*b*|	34.41757	5.80025	6.28753	28.25720	48.20414
CT(1 → 2) - CT(2 → 1)	0.78610	0.61200	0.67540	0.78440	0.53030
DMSO					
Frag.1 → Frag.2 donation (*d*)	0.29691	0.17013	0.22975	0.35872	0.32508
Frag.1 ← Frag.2 back donation (*b*)	−0.00853	0.02883	0.03608	−0.01240	0.00691
Net Frag.1 → Frag.2 donation (*d*-*b*)	0.30544	0.14130	0.19367	0.37112	0.31817
Donation to back donation ratio, |*d*/*b*|	34.82839	5.90087	6.36797	28.93394	47.05196
CT(1 → 2) - CT(2 → 1)	0.79060	0.61670	0.68310	0.79150	0.53290

[a]Frag. refers to fragment, where Frag.1 is L1 and Frag.2 is MCl_2 [M = Ni(II), Pd(II), Pt(II), Cu(II), and Zn(II)].
[b]The overall results for alpha and beta electrons are reported for the Cu(II) chloride complex of L1.

temperature, and concentration [38], the switchable NLO response of MAPTSC can be easily fine-tuned by modifying these factors.

The coordination of L1 to different transition metal centers results in significant modifications of its β_{tot} value. Further modifications of this value are observed in the presence of bulk solvents especially the highly polar ones. Therefore, the first hyperpolarizability vis-a-vis the second-order NLO response of L1 can be highly tuned by coordination to different transition metal ions and by the presence of solvents with different dielectric constants. The complexation of L1 with Zn(II) and Pt(II) chlorides results in a modest to drastic increments of its gas-phase β_{tot} value, respectively. Unexpectedly, the complexation of L1 with Ni(II), Pd(II), and Cu(II) chlorides reduced its β_{tot} value. This is unexpected because electronic transitions involving metal-based orbitals in these complexes are supposed to reinforce their optical nonlinearities.

It is clear from the β_{tot} values in Table 2 and the graphs in Figure 3 that the presence of a bulk solvent strengthens the first hyperpolarizability thereby reinforcing the second-order NLO response of each molecule studied to a greater or lesser extent, depending on solvent polarity. In fact, the β_{tot} values of these molecules when present in the nonpolar solvent (benzene) and in the polar solvents (ethanol and DMSO) are larger than the corresponding gas-phase values by factors in the ranges 2.7–13.1 and 3.5–58.6, respectively. Exceptionally, the β_{tot} value for the Pt(II) chloride complex in benzene dropped below the gas-phase value by a factor of about 5. Based on our β_{tot} values, it is clear that all of the molecules investigated are likely to exhibit their greatest second-order NLO activities in DMSO, which has the largest dielectric constant among the solvents used. Consequently, further discussion pertaining to solvent effects on β_{tot} and second-order NLO properties of MAPTSC and its complexes has been restricted to the results obtained in DMSO. As clearly shown by the graphs in Figure 3, the magnitudes of the β_{tot} values of the molecules studied are in the order $[Pd(L1)Cl_2] < [Ni(L1)Cl_2] < [Cu(L1)Cl_2] < L1 < [Zn(L1)Cl_2] < [Pt(L1)Cl_2]$ in vacuum and $[Pt(L1)Cl_2] < L1 < [Ni(L1)Cl_2] < [Zn(L1)Cl_2] < [Pd(L1)Cl_2] < [Cu(L1)Cl_2]$ in DMSO.

To determine the plausible CT mechanisms responsible for the first hyperpolarizabilities and hence quadratic NLO activities of the molecules investigated, the relationship between the frontier molecular orbitals (HOMO-LUMO) energy gaps and the β_{tot} values has been scrutinized. Since transition metals are capable of inducing low-energy MLCT and LMCT transitions that can greatly contribute to the first

Table 2: β_{tot}, β_x, β_y, and β_z values of MAPTSC and the complexes calculated at B3LYP/6-31++G(d,p)/(SDD for metal ions) and B3LYP/6-311++G(d,p)/(SDD for metal ions) levels of theory in different media.

Basis set	6-31++G(d,p)/(SDD for metal ions)				6-311++G(d,p)/(SDD for metal ions)			
Molecule	β_x(a.u.)	β_y(a.u.)	β_z(a.u.)	$\beta_{tot} \times 10^{-30}$ (esu)	β_x(a.u.)	β_y(a.u.)	β_z(a.u.)	$\beta_{tot} \times 10^{-30}$ (esu)
				Gas-phase				
L1	814.59	198.71	103.02	7.298	731.74	184.26	114.38	6.594
L2	1056.16	−724.81	−60.49	11.079	1016.92	−700.38	−46.18	10.675
$[Ni(L1)Cl_2]$	331.18	−506.92	409.83	6.317	463.27	−528.93	420.36	7.077
$[Pd(L1)Cl_2]$	315.26	−366.04	431.49	5.596	454.30	−382.74	448.43	6.430
$[Pt(L1)Cl_2]$	1460.79	−444.13	502.44	13.887	1635.25	−452.82	521.00	15.334
$[Cu(L1)Cl_2]$	−675.03	−363.16	36.41	6.630	−560.28	−376.66	43.37	5.845
$[Zn(L1)Cl_2]$	−811.24	−390.90	345.28	8.332	−706.61	−389.50	361.74	7.639
				Benzene				
L1	1282.49	56.10	167.35	11.184	1179.22	45.43	174.07	10.306
L2	1551.36	−1089.99	−89.36	16.398	1502.70	−1060.86	−70.78	15.903
$[Ni(L1)Cl_2]$	−823.01	−357.05	543.42	9.062	−666.92	−391.48	557.98	8.239
$[Pd(L1)Cl_2]$	939.71	−327.52	−637.52	10.210	773.32	−357.51	−660.79	9.315
$[Pt(L1)Cl_2]$	−573.09	−407.87	−744.78	8.850	−785.46	−425.23	−769.99	10.188
$[Cu(L1)Cl_2]$	−2260.96	−238.64	184.96	19.706	−2117.62	−256.13	197.51	18.507
$[Zn(L1)Cl_2]$	−1606.20	−364.44	316.52	14.489	−1495.75	−365.53	330.97	13.606
				Ethanol				
L1	2137.32	−269.15	147.01	18.654	2024.98	−291.42	158.79	17.728
L2	2267.08	−1677.29	−143.98	24.395	2205.02	−1645.93	−119.16	23.794
$[Ni(L1)Cl_2]$	−3142.76	−179.82	920.82	28.335	−2956.62	−233.21	947.43	26.898
$[Pd(L1)Cl_2]$	3594.07	−415.42	−1047.59	32.541	3379.29	−475.21	−1083.34	30.932
$[Pt(L1)Cl_2]$	1657.19	−276.44	−1112.58	17.409	1397.74	−309.05	−1150.21	15.865
$[Cu(L1)Cl_2]$	−7509.45	−198.28	712.29	65.190	−7206.75	−225.86	739.63	62.619
$[Zn(L1)Cl_2]$	−3310.72	−198.42	547.88	29.042	−3182.29	−203.79	582.65	28.005
				DMSO				
L1	2206.37	−303.91	144.37	19.282	2094.06	−325.95	156.44	18.359
L2	2315.01	−1719.20	−147.47	24.945	2251.91	−1687.90	−122.31	24.336
$[Ni(L1)Cl_2]$	−3329.44	−163.94	955.14	29.958	−3140.90	−219.30	982.93	28.496
$[Pd(L1)Cl_2]$	−3565.27	−417.46	935.93	32.049	−3351.90	−483.07	969.63	30.433
$[Pt(L1)Cl_2]$	1848.88	−258.57	−1142.88	18.911	1585.59	−292.58	−1181.51	17.269
$[Cu(L1)Cl_2]$	−8098.75	−202.43	757.49	70.295	−7773.97	−230.92	783.55	67.531
$[Zn(L1)Cl_2]$	−3437.58	−176.12	553.46	30.119	−3308.23	−181.74	588.93	29.073

hyperpolarizability of MAPTSC, photoinduced electronic transitions in the molecules have been studied via the TD-DFT method. Changes in the gas-phase β_{tot} value for L1 as a result of L1–MCl_2 binding are attributed solely to the effects of the different transition metal ions present in the MCl_2 fragment. Such changes in the presence of both the MCl_2 fragment and the bulk solvent are attributable to the concomitant effects of metallation and solvent polarity.

3.3. First Molecular Hyperpolarizabilities and HOMO-LUMO Energy Analysis. The HOMO-LUMO energy gaps ($\Delta E_{H\text{-}L}$) of L1 and its transition metal chloride complexes, computed at B3LYP/6-31++G(d,p)/(SDD for metal ions) level of theory in gas-phase and in DMSO are listed in Table 3. The $\Delta E_{H\text{-}L}$ values for the Cu(II) chloride complex of L1 in both media have been calculated from the eigenvalues of the beta spin orbitals, because a majority of its electronic transitions (analyzed in the next section) involve these orbitals. The D-π-A or push-pull CT mechanism predominates in molecules when an inverse proportionality relationship exists between their $\Delta E_{H\text{-}L}$ and β_{tot} values. The push-pull mechanism is strongly dependent on HOMO-LUMO energy gaps because a proper electronic conjugation must exist among the molecular orbitals of a system for ICT to be effective [7]. The relationship between the gas-phase $\Delta E_{H\text{-}L}$ and β_{tot} values of the molecules studied is far from being inversely proportional, implying that the D-π-A push-pull process is not the dominant CT mechanism in each of the molecules in gas-phase. Photoinduced electronic transitions with CT character (involving metal-based orbitals) are certainly playing the dominant role.

Table 3: HOMO/LUMO energies and β_{tot} values of MAPTSC and its metal chloride complexes computed in gas-phase and DMSO at B3LYP/6-31++G(d,p)/(SDD for metal ions) level of theory.

Molecule	Energies in gas-phase (eV)			$\beta_{tot} \times 10^{-30}$ (esu)	Energies in DMSO (eV)			$\beta_{tot} \times 10^{-30}$ (esu)
	HOMO[a] energy	LUMO[b] energy	$\Delta E_{H\text{-}L}$[c]		HOMO[a] energy	LUMO[b] energy	$\Delta E_{H\text{-}L}$[c]	
L1	−5.481	−1.189	4.292	7.298	−6.134	−1.334	4.801	19.282
$[Ni(L1)Cl_2]$	−5.815	−2.397	3.418	6.317	−6.589	−2.797	3.791	29.958
$[Pd(L1)Cl_2]$	−5.895	−2.496	3.399	5.596	−6.574	−3.010	3.564	32.049
$[Pt(L1)Cl_2]$	−5.715	−2.386	3.329	13.887	−6.272	−2.350	3.923	18.911
$[Cu(L1)Cl_2]$	−6.240	−3.575	2.665	6.630	−6.723	−4.043	2.679	70.295
$[Zn(L1)Cl_2]$	−6.744	−2.193	4.551	8.332	−6.621	−2.014	4.607	30.119

[a]HOMO stands for highest occupied molecular orbital.
[b]LUMO stands for lowest unoccupied molecular orbital.
[c]$\Delta E_{H\text{-}L}$ represents HOMO-LUMO energy gap.

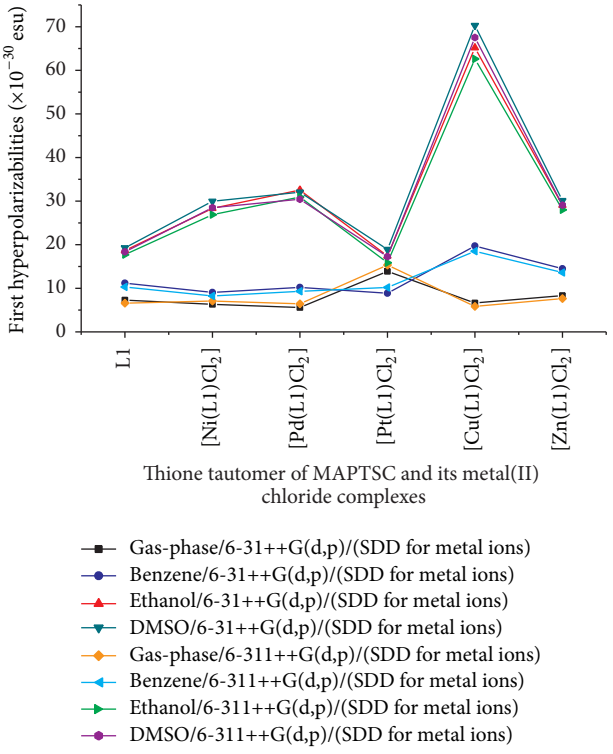

Figure 3: Trends in β_{tot} values of L1 and its transition metal chloride complexes from gas to solvent phases.

In DMSO, a somewhat inverse proportionality relationship is found between the values of $\Delta E_{H\text{-}L}$and β_{tot}, suggesting that CT in these molecules is due to the combined effects of photoinduced electronic transitions with CT character and the D-π-A push-pull process. The polar solvent medium therefore enhances charge transfer in each of the molecules investigated.

3.4. Electronic Absorption Spectra of L1 and Its Transition Metal Chloride Complexes. In order to determine the optical transparency of each investigated molecule in the visible region of the EM spectrum and to determine the electronic transitions with CT character, the UV-Vis spectra of these molecules were simulated via TD-DFT studies. To study solvatochromic effects, the UV-Vis spectra were calculated in both gas-phase and DMSO. For each molecule, electronic transitions to the first 10 low-lying singlet excited states were studied at CAM-B3LYP/6-31++G(d,p)/(SDD for metal ions) level of theory. The computed electronic excitation energies (ΔE in eV), wavelengths (λ in nm), and oscillator strengths (f) are presented in Table 4. The electronic transitions with oscillator strengths 0.02 and above have been considered, since those with very low oscillator strengths are likely to make insignificant contributions to the first hyperpolarizabilities of the molecules studied. The UV-Vis spectra of these molecules in gas and solvent phases are presented in Figure 4.

The modification undergone by the β_{tot} value for L1 upon complexation with different transition metal chlorides appears to be related to the types and intensities (oscillator strengths) of the electronic excitations in the complexes formed. The reduction in the β_{tot} value for L1 following its complexation with Ni(II), Pd(II), and Cu(II) chlorides in vacuo is apparently linked to the reduction in the number of electronic transitions in the resulting complexes, coupled with a decrease in the oscillator strengths of the transitions. Although complexation leads to a slight lowering of the electronic excitation energies of the dominant electronic transitions in the complexes $[Ni(L1)Cl_2]$, $[Pd(L1)Cl_2]$, and $[Cu(L1)Cl_2]$, a corresponding increase in their β_{tot} values is not observed. This is probably due to the significant intensity reduction of these transitions relative to those in L1. On the contrary, the complexation of L1 with the Pt(II) chloride in vacuum results in a dramatic increment of the ligand's gas-phase β_{tot} value, which can be attributed to the introduction of several low-energy intense electronic transitions.

By inspection of Figure 4 and Table 4, it can be seen that the number of reasonably strong electronic transitions in the molecules studied increases significantly in DMSO. Moreover, the polar DMSO medium leads to a modest lowering of the excitation energies of the dominant electronic transitions in all complexes investigated, except the Pt(II) chloride complex. Therefore, the $[Ni(L1)Cl_2]$, $[Pd(L1)Cl_2]$, $[Cu(L1)Cl_2]$,

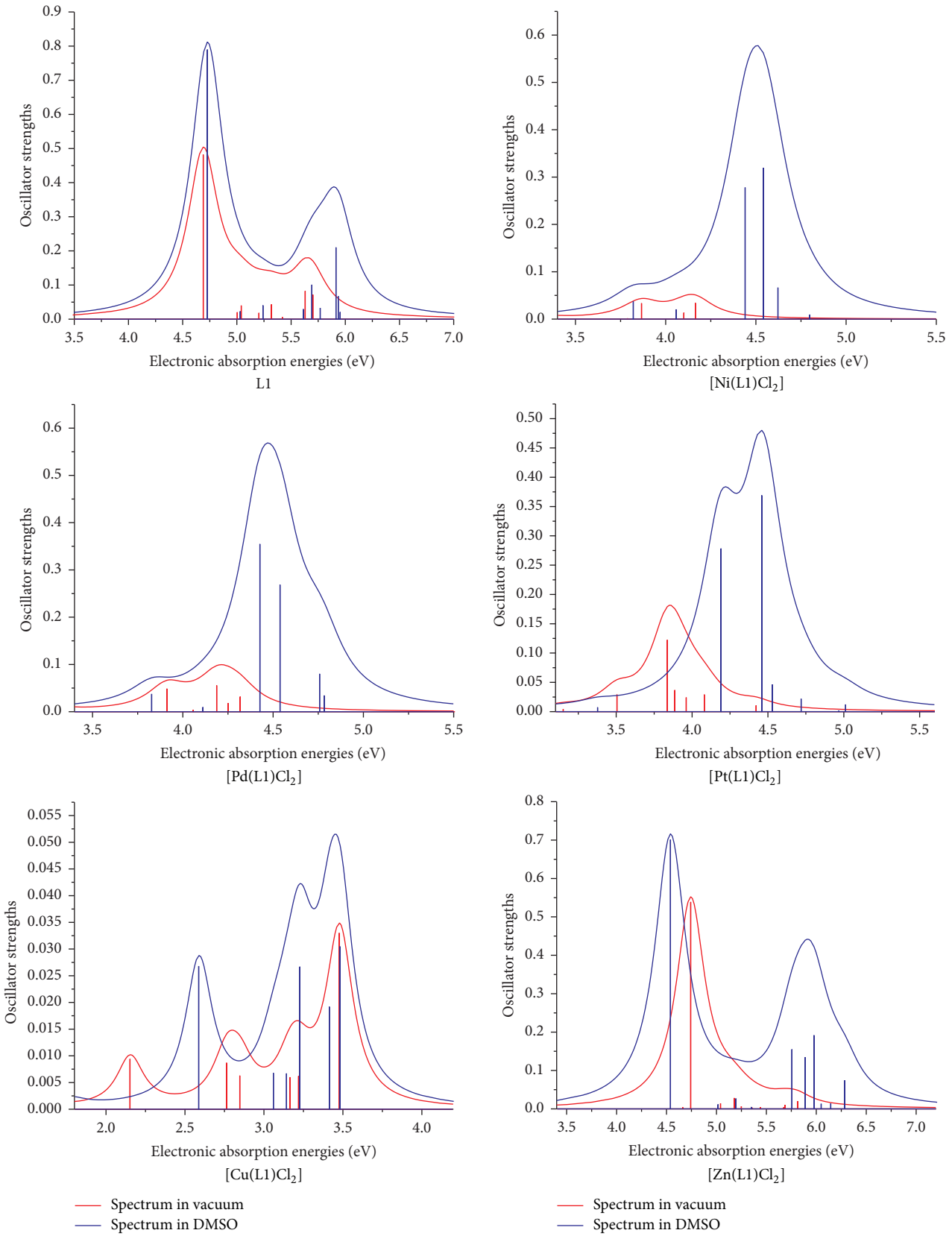

Figure 4: The electronic absorption spectra of L1 and its complexes in gas-phase and DMSO computed at CAM-B3LYP/6-31++G(d,p)/(SDD for metal ions) level of theory.

Table 4: Absorption energies (E, eV), wavelengths (λ, nm), and oscillator strengths (f) of L1 and the complexes, calculated at CAM-B3LYP/6-31++G(d,p)/(SDD for metal ions) level of theory in gas-phase and DMSO by the TD-DFT method.

Molecule	Gas-phase				DMSO			
	State	ΔE (eV)	λ (nm)	f	State	ΔE (eV)	λ (nm)	f
L1	**S2**	**4.6892**	**264.40**	**0.4821**	**S2**	**4.7279**	**262.24**	**0.7898**
	S3	5.0039	247.77	0.0203	S3	5.0309	246.44	0.0231
	S4	5.0404	245.98	0.0401	S4	5.2409	236.57	0.0406
	S6	5.3192	233.09	0.0435	S5	5.6131	220.88	0.0294
	S8	5.6300	220.22	0.0826	S6	5.6917	217.83	0.1009
	S10	5.7011	217.47	0.0717	S7	5.7689	214.92	0.0329
					S8	5.9143	209.63	0.2104
					S9	5.9352	208.90	0.0676
					S10	5.9525	208.29	0.0210
$[Ni(L1)Cl_2]$	S7	3.8661	320.70	0.0336	S5	3.8202	324.55	0.0377
	S9	**4.1644**	**297.73**	**0.0342**	S6	4.0588	305.47	0.0206
					S7	4.4403	279.23	0.2780
					S8	**4.5408**	**273.04**	**0.3197**
					S9	4.6220	268.25	0.0666
$[Pd(L1)Cl_2]$	S6	3.9119	316.94	0.0488	S5	3.8273	323.95	0.0376
	S8	**4.1873**	**296.10**	**0.0557**	**S7**	**4.4265**	**280.10**	**0.3549**
	S10	4.3174	287.17	0.0320	S8	4.5383	273.20	0.2687
					S9	4.7574	260.61	0.0802
					S10	4.7830	259.22	0.0345
$[Pt(L1)Cl_2]$	S5	3.5049	353.75	0.0293	S5	4.1907	295.85	0.2784
	S6	**3.8361**	**323.20**	**0.1224**	**S6**	**4.4592**	**278.04**	**0.3691**
	S7	3.8860	319.05	0.0368	S7	4.5295	273.72	0.0466
	S8	3.9611	313.00	0.0243	S8	4.7188	262.75	0.0219
	S9	4.0806	303.84	0.0292				
$[Cu(L1)Cl_2]$	**S10**	**3.4788**	**356.40**	**0.0330**	S5	2.5892	478.86	0.0268
					S8	3.2291	383.96	0.0267
					S10	**3.4829**	**355.98**	**0.0305**
$[Zn(L1)Cl_2]$	**S2**	**4.7424**	**261.44**	**0.5390**	**S1**	**4.5399**	**273.10**	**0.7015**
	S4	5.1784	239.43	0.0285	S3	5.1949	238.67	0.0271
	S10	5.8132	213.28	0.0202	S5	5.7561	215.39	0.1552
					S6	5.8884	210.56	0.1346
					S7	5.9773	207.43	0.1919
					S10	6.2838	197.31	0.0746

and $[Zn(L1)Cl_2]$ complexes must possess highly polar excited states that are greatly solvated and stabilized by the polar DMSO molecules, whereas their ground states are less polar and hence less stabilized by solvation. Consequently, excitation energies from the less stabilized ground states to the highly stabilized excited states are reduced, leading to an increase in the number of intense electronic excitations in the complexes. This in turn causes a dramatic increment in the β_{tot} values of the complexes in DMSO as solvent, thus enhancing their quadratic NLO responses. Strong absorption of light in the visible region of the EM spectrum restricts the NLO applications of materials [39] due to significant transparency/nonlinearity trade-offs that often lead to lower device efficiency and reduced photostability. From Figure 4, it can be seen that, apart from the $[Cu(L1)Cl_2]$ complex, all investigated molecules have high optical transparencies in the entire visible region, implying that they suffer very low optical losses. Hence, transparency/nonlinearity trade-offs are highly minimized in L1 and its Ni(II), Pd(II), Pt(II), and Zn(II) chloride complexes, confirming their suitability for the fabrication of NLO devices.

To decipher the relationship between solvent polarity and the first hyperpolarizabilities of the molecules studied, their UV-Vis spectra in gas-phase and in DMSO have been compared as shown in Figure 4. It is clear from Figure 3 that polar solvents substantially increase the β_{tot} value for the Cu(II) chloride complex of L1 but have almost no effect on the β_{tot} value for the Pt(II) chloride complex. The effects of the polar solvents on the β_{tot} values for these molecules have been explained in terms of the solvatochromic shift directions of their strongest electronic transitions on going from the gas-phase to the DMSO solvent medium, as elucidated in

Figure 4. The drastic increment in the β_{tot} value for the Cu(II) chloride complex in DMSO is ascribed to its positive solvatochromism (the shift of its strongest CT absorption bands towards lower excitation energies and longer wavelengths). The remarkable negative solvatochromism exhibited by the Pt(II) chloride complex in DMSO (the shift of its strongest CT absorption bands towards higher excitation energies and shorter wavelengths) accounts for the insignificant modification of its β_{tot} value in the polar solvents. The positive solvatochromism (bathochromic or red-shift of the strongest CT absorption bands) exhibited by the $[Zn(L1)Cl_2]$ complex is responsible for the increment in its β_{tot} value in DMSO. Solvatochromism as such is not obvious from the comparison of the gas and solvent phase UV-Vis spectra of L1 in Figure 4. The increment in its β_{tot} value in DMSO is certainly linked to the increase in the intensities of its strong electronic excitations. Although the complexes $[Ni(L1)Cl_2]$ and $[Pd(L1)Cl_2]$ display a certain degree of negative solvatochromism in DMSO (hypsochromic or blue-shift of their strongest CT absorption bands), appreciable increments in their β_{tot} values are observed due to significant contributions from strong low-lying electronic transitions of CT character to their first hyperpolarizabilities.

By comparing the gas-phase UV-Vis absorption spectra of ligand L1 with those of its metal chloride complexes, it is clear that metallation results in significant modifications of the ligand's electronic absorption spectrum. These modifications are caused by the introduction of CT bands induced by the promotion of electrons from orbitals that are predominantly metal in character to orbitals that are predominantly ligand in character (MLCT), or the reverse (LMCT). These CT bands generally give significant contributions to the first molecular hyperpolarizability. Such CT transitions are absent from the UV-Vis spectrum of the Zn(II) chloride complex because the *d*-orbitals of the Zn(II) ion are fully filled and do not participate in electronic transitions.

The dominant electronic transitions of the molecules studied (those with the greatest oscillator strengths) have been characterized via natural transition orbital (NTO) analysis which generates unique "particle-hole" NTO pairs from the canonical molecular orbitals. Only the dominant electronic transitions (those boldly highlighted in Table 4) have been characterized because they are capable of remarkable contributions to the first molecular hyperpolarizability. For each "particle-hole" NTO pair, the "particle" shows where in the system electrons come from and the "hole" indicates where the electrons go to, during electronic transitions. The NTOs of the molecules studied (shown in Table 5) were computed using Gaussian 09W and then rendered with VMD 1.9.2 [40] using isosurface cube files generated by Multiwfn 3.3.8. To obtain a quantitative description of the NTOs, orbital contributions from different molecular fragments (reported in Table 6) were calculated using the orbital composition analysis option [41] of Multiwfn 3.3.8. These orbital compositions, together with the electronic distributions of the NTOs (depicted by their isosurfaces in Table 5) were exploited in characterizing the dominant electronic transitions of the molecules studied. These transitions along with their most probable characters are listed in Table 7.

The qualitative and quantitative analyses of the NTOs have revealed photoinduced electronic transitions with CT character in the UV-Vis spectra of the molecules. In gas-phase, the "particle" of L1 is predominantly contributed by lone pair orbitals (n) located on the sulfur and nitrogen atoms in the TSC moiety, while the corresponding "hole" is fairly distributed over the entire molecule and is dominated by π^*-antibonding character. This implies that $n \rightarrow \pi^*$ electronic transitions predominate in the gas-phase ligand. The "particle" and "hole" of L1 in DMSO are both distributed over the entire molecular framework. While the "particle" is comprised of n and π-type orbitals, the "hole" is dominated by π^*-type orbitals. Therefore, both $n \rightarrow \pi^*$ and $\pi \rightarrow \pi^*$ electronic transitions are possible in the ligand when present in DMSO as solvent. The DMSO environment thus enhances CT in L1 giving rise to the dramatic increment of its β_{tot} value. The complexation of L1 with different transition metal chlorides introduces new electronic transitions with CT character in the electronic spectrum of L1 and/or modifies the existing ones, owing to the presence of low-lying metal-based orbitals. It is evidenced in Tables 5 and 7 that the dominant electronic transitions in the metal chlorides complexes of L1 studied (except the Zn(II) chloride complex) are dominated by MLCT and/or LMCT electronic transitions, along with LLCT transitions. The introduction of MLCT and LMCT electronic transitions often, but not always, bolsters the first molecular hyperpolarizabilities of organic push-pull systems, as observed in the present study. From the foregoing, the NLO response of MAPTSC can be highly tuned by transition metal chelation.

The complexation of L1 with the Ni(II), Pd(II), Pt(II), and Cu(II) chlorides in vacuo leads to "partial resonance" or loss of conjugation in the benzene rings of the "particle" NTOs of the resulting complexes (see Table 5). Consequently, ICT in these complexes derived from donor-acceptor electron cloud movement across the π-conjugated pathway is disrupted in vacuo. As such, the D-π-A or push-pull CT process is unlikely to occur in the gas-phase complexes. Nevertheless, the electronic transitions with CT character MLCT, LMCT, and LLCT do occur in these complexes accounting for their first hyperpolarizabilities. The scenario in the gas-phase Zn(II) chloride complex is opposite to that in the aforementioned complexes because π-conjugation is rather reinforced in the benzene rings of both the "particle" and the "hole," whereas MLCT, LMCT, and LLCT electronic transitions are prohibited. This implies that CT in this complex is almost entirely due to the push-pull mechanism. The absence of the metal-based transitions MLCT and LMCT from the UV-Vis spectrum of the $[Zn(L1)Cl_2]$ complex is attributed to the nonparticipation of the fully filled *d*-orbitals of the Zn(II) ion in electronic transitions. It is clear from the isosurfaces in Table 5 that π-conjugation is unhindered in the benzene rings of the "particle" NTOs of the complexes when present in the DMSO solvent medium. This significantly strengthens their push-pull CT mechanisms, resulting in dramatic first hyperpolarizability increments. It is found that as solvent polarity increases, ICT in the Ni(II), Pd(II), Pt(II), and Cu(II) chlorides complexes of L1 increases, and their first hyperpolarizabilities are increasingly contributed by a synergy of

Table 5: The dominant NTO "particle-hole" pairs for the dominant electronic transitions of each investigated molecule in gas-phase and in DMSO.

Molecule	Gas-phase		DMSO	
	Particle	Hole	Particle	Hole
L1	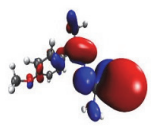	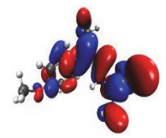	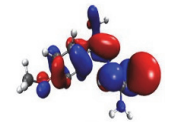	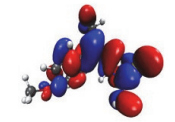
[Ni(L1)Cl_2]	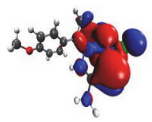	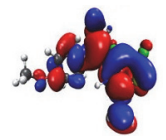	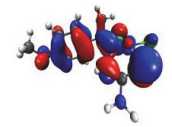	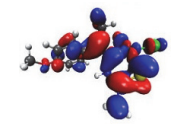
[Pd(L1)Cl_2]	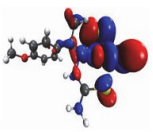	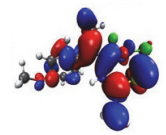	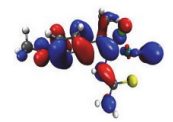	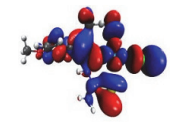
[Pt(L1)Cl_2]	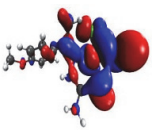	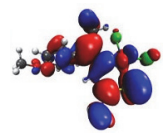	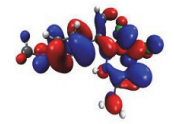	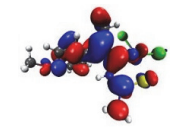
[Cu(L1)Cl_2]	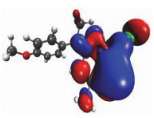	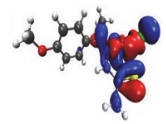	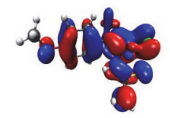	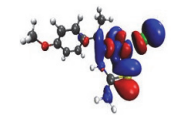
[Zn(L1)Cl_2]	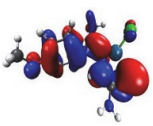	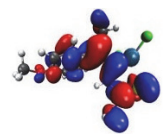	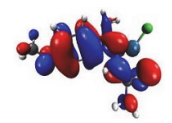	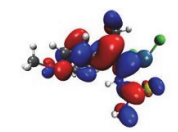

electronic transitions with CT character (MLCT, LMCT, and LLCT) and the donor-acceptor electron cloud movements across intervening π-conjugation paths. Exceptionally, ICT in the Zn(II) chloride complex is found to occur entirely via the push-pull mechanism in both gas and solvent phases.

3.5. Natural Bond Orbital (NBO) Analysis. To gain a deeper insight into the nature of conjugative and hyperconjugative interactions responsible for electron delocalization and ICT in L1 and its complexes, natural bond orbital (NBO) analyses have been carried out on the molecules studied using the NBO 3.1 [42] module embedded in Gaussian 09W. The NBO results are presented in Tables 8 and 9. The delocalization of electron density (ED) between occupied Lewis-type (bonding or lone pair) natural bond orbitals (NBOs) and formally unoccupied non-Lewis NBOs (antibonds or Rydberg) correspond to stabilizing donor-acceptor interactions. The stabilization energy, $E^{(2)}$, that results from the interaction of a donor (i) and an acceptor (j) NBO pair is estimated by means of the second-order perturbation theory as shown in (5). The values of $E^{(2)}$ are proportional to the extent of conjugation. Hence, the larger the $E^{(2)}$ value, the more intensive the donor-acceptor NBO interaction and the larger the ICT that occurs in the entire system [23, 43].

$$E_{ij}^{(2)} = -q\frac{\left(\widehat{F}_{ij}\right)^2}{\varepsilon_j - \varepsilon_i}, \tag{5}$$

where q is the donor orbital occupancy, ε_i and ε_j are diagonal elements (orbital energies) of donor and acceptor NBOs, respectively, and $\widehat{F}_{ij}$ is the off-diagonal NBO Fock matrix element. In molecular systems, π-conjugation results from π-electron delocalization due to $\pi \rightarrow \pi^*$ interactions. While primary hyperconjugation is due to $\sigma \rightarrow \pi^*$, $n \rightarrow \pi^*$, $n \rightarrow \sigma^*$, or $\pi^* \rightarrow \pi^*$ interactions, secondary hyperconjugation occurs as a result of $\sigma \rightarrow \sigma^*$ interactions [11]. The NBO interactions LP(2)O2 $\rightarrow \pi^*$(C6-C7), LP(1)O2 $\rightarrow \pi^*$(C6-C11), or LP(2)O2 $\rightarrow$ LP*(1)C6, with $E^{(2)}$ values in the range 16.04–59.60 kcal/mol have clearly confirmed that the $-OCH_3$ group is the electron donor in all of the D-π-A or push-pull systems studied. Intensive $\pi \rightarrow \pi^*$ conjugative interactions dominate in the benzene rings of all molecules studied, greatly enhancing their CT capabilities and optical nonlinearities. The π-conjugated pathway for the D-π-A structure of each

Table 6: Natural transition orbitals (NTOs) compositions for the thione tautomer of MAPTSC and its complexesin gas-phase and DMSO, calculated at the TD-DFT/CAM-B3LYP/6-31++G(d,p)/(SDD for metal ions) level of theory.

Molecule	NTOs	Orbital compositions of fragments (%)				Main distribution of NTOs on molecular systems
		M(II)[a]	MAP[b]	TSC[c]	$2Cl^-$	
				Gas-phase		
L1	Hole	—	36.496	63.504	—	MAP + TSC
	Particle	—	13.856	86.144	—	TSC
$[Ni(L1)Cl_2]$	Hole	4.537	50.724	43.388	1.351	MAP + TSC
	Particle	46.092	2.627	9.700	41.581	Ni(II) ion + $2Cl^-$
$[Pd(L1)Cl_2]$	Hole	3.958	49.695	45.108	1.239	MAP + TSC
	Particle	32.732	4.901	6.195	56.172	Pd(II) ion + $2Cl^-$
$[Pt(L1)Cl_2]$	Hole	5.517	43.596	49.385	1.501	MAP + TSC
	Particle	56.516	5.890	7.933	29.661	Pt(II) ion + $2Cl^-$
$[Cu(L1)Cl_2]$	Hole	59.034	3.915	11.890	25.160	Cu(II) ion + $2Cl^-$
	Particle	8.056	3.214	66.050	22.679	TSC + $2Cl^-$
$[Zn(L1)Cl_2]$	Hole	1.873	45.358	51.649	1.119	MAP + TSC
	Particle	1.731	34.905	57.951	5.413	MAP + TSC
				DMSO		
L1	Hole	—	41.677	58.323	—	MAP + TSC
	Particle	—	29.818	70.182	—	MAP + TSC
$[Ni(L1)Cl_2]$	Hole	19.896	37.686	36.486	5.932	Ni(II) ion + MAP + TSC
	Particle	6.189	40.681	35.610	17.520	MAP + TSC + $2Cl^-$
$[Pd(L1)Cl_2]$	Hole	34.365	25.958	24.693	14.984	Pd(II) ion + MAP + TSC + $2Cl^-$
	Particle	1.806	61.076	23.100	14.018	MAP + TSC + $2Cl^-$
$[Pt(L1)Cl_2]$	Hole	5.065	60.271	33.556	1.108	MAP + TSC
	Particle	30.291	52.437	12.099	5.173	Pt(II) ion + MAP
$[Cu(L1)Cl_2]$	Hole	61.952	2.016	17.871	18.162	Cu(II) ion + TSC + $2Cl^-$
	Particle	9.275	22.645	20.973	47.107	MAP + TSC + $2Cl^-$
$[Zn(L1)Cl_2]$	Hole	1.932	61.449	35.673	0.945	MAP + TSC
	Particle	0.714	70.615	27.791	0.880	MAP + TSC

[a]M(II) represents the transition metal ions.
[b]MAP is the 4-methoxyacetophenone moiety.
[c]TSC is the thiosemicarbazones moiety.

Table 7: Excitation energies and wavelengths, oscillator strengths, NTO eigenvalues, and characters of the dominant electronic transitions for MAPTSC and its complexesin gas-phase and DMSO, calculated at the TD-DFT/CAM-B3LYP/6-31++G(d,p)/(SDD for metal ions) level of theory.

Medium	Molecule	Excited state	Electronic transition[a]	NTO eigenvalue	f	ΔE (eV)	λ_{max} (nm)	Character[b]
Gas-phase	L1	2	P → H	0.8866	0.4821	4.6892	264.40	$n \rightarrow \pi^*$
	$[Ni(L1)Cl_2]$	9	P → H	0.9299	0.0342	4.1644	297.73	MLCT/LLCT
	$[Pd(L1)Cl_2]$	8	P → H	0.9261	0.0557	4.1873	296.10	MLCT/LLCT
	$[Pt(L1)Cl_2]$	6	P → H	0.9731	0.1224	3.8361	323.20	MLCT/LLCT
	$[Cu(L1)Cl_2]$	10	P → H	1.6191	0.0330	3.4788	356.40	LMCT/LLCT
	$[Zn(L1)Cl_2]$	2	P → H	0.9265	0.5390	4.7424	261.44	ILCT
DMSO	L1	2	P → H	0.9190	0.7898	4.7279	262.24	$n \rightarrow \pi^*/\pi \rightarrow \pi^*$
	$[Ni(L1)Cl_2]$	8	P → H	0.6493	0.3197	4.5408	273.04	LMCT/ILCT/LLCT
	$[Pd(L1)Cl_2]$	7	P → H	0.8746	0.3549	4.4265	280.10	LMCT/ILCT/LLCT
	$[Pt(L1)Cl_2]$	6	P → H	0.9330	0.3691	4.4592	278.04	MLCT/ILCT
	$[Cu(L1)Cl_2]$	10	P → H	1.7312	0.0305	3.4829	355.98	LMCT/ILCT/LLCT
	$[Zn(L1)Cl_2]$	1	P → H	0.9575	0.7015	4.5399	273.10	ILCT

[a]P stands for "*particle*" and H stands for "*hole.*"
[b]n represents occupied lone pair orbitals.

Table 8: Significant second-order interaction energies ($E^{(2)}$, kcal/mol) between donor and acceptor NBOs of L1 and its Cu(II) and Zn(II) chloride complexes.

L[a]	$E^{(2)}$ (kcal/mol)		$[Cu(L1)Cl_2]$[a]	$E^{(2)}$(kcal/mol)[b]		$[Zn(L1)Cl_2]$[a]	$E^{(2)}$ (kcal/mol)	
Donor(i) → acceptor(j)	Gas-phase	DMSO	Donor(i) → acceptor(j)	Gas-phase	DMSO	Donor(i) → acceptor(j)	Gas-phase	DMSO
π(C6-C7) → π^*(C8-C9)	22.85	23.77	π(C6-C7) → π^*(C8-C9)	12.11 (12.21)	12.77 (12.90)	π(C6-C11) → π^*(C7-C8)	17.82	16.94
π(C6-C7) → π^*(C10-C11)	16.59	16.60	π(C6-C7) → π^*(C10-C11)	8.15 (8.08)	8.13 (8.03)	π(C6-C11) → π^*(C9-C10)	25.30	26.24
π(C8-C9) → π^*(C6-C7)	17.00	16.69	π(C8-C9) → π^*(C6-C7)	8.08 (8.02)	7.94 (7.91)	π(C7-C8) → π^*(C6-C11)	22.81	23.24
π(C8-C9) → π^*(C10-C11)	21.53	21.77	π(C8-C9) → π^*(C10-C11)	10.56 (10.61)	10.71 (10.74)	π(C7-C8) → π^*(C9-C10)	17.03	16.60
π(C10-C11) → π^*(C6-C7)	21.19	21.28	π(C10-C11) → π^*(C6-C7)	10.54 (10.59)	10.54 (10.60)	π(C9-C10) → π^*(C6-C11)	17.79	17.12
π(C10-C11) → π^*(C8-C9)	17.49	17.13	π(C10-C11) → π^*(C8-C9)	8.63 (8.57)	8.36 (8.30)	π(C9-C10) → π^*(C7-C8)	23.27	22.73
LP(2)O2 → π^*(C6-C7)	30.64	30.75	π(S25-Cu29) → LP*(1)C24	(150.08)	—	**π(C9-C10) → π^*(C16-N21)**	**3.05**	**10.62**
LP(1)N21 → σ^*(C9-C16)	**11.68**	**11.15**	σ^*(S25-Cu29) → LP*(5)Cu29	(1.22)	(24.74)	**π^*(C16-N21) → π^*(C9-C10)**	—	**34.19**
LP(1)N22 → π^*(C16-N21)	*25.75*	*23.29*	**π^*(C16-N21) → π^*(C8-C9)**	**23.05 (23.93)**	**14.34 (14.73)**	LP(2)O2 → π^*(C6-C11)	28.78	29.21
LP(1)N22 → LP(1)C24*	—	*130.14*	LP(2)O2 → π^*(C6-C7)	16.04 (16.11)	16.10 (16.20)	LP(1)N21 → LP*(6)Zn29	23.71	31.05
LP(1)N22 → σ^*(C24-S25)	*48.42*	—	LP(1)N21 → LP*(5)Cu29	(27.57)	—	LP(1)N21 → LP*(9)Zn29	28.64	30.63
LP(2)S25 → σ^*(N22-C24)	*13.92*	*11.69*	LP(1)N21 → LP*(6)Cu29	12.23	16.4 (37.24)	*LP(1)N22 → LP*(1)C24*	*128.39*	*135.41*
LP(3)S25 → LP(1)C24*	—	*212.55*	LP(1)N21 → LP*(8)Cu29	10.74	18.42	LP(1)N22 → π^*(C16-N21)	22.05	20.45
LP(2)S25 → σ^*(C24-N26)	*11.37*	*9.33*	LP(1)N21 → LP*(9)Cu29	10.42	7.47	LP(1)S25 → LP*(7)Zn29	0.55	17.41
LP(1)N26 → LP(1)C24*	—	*137.34*	*LP(1)N22 → π^*(C16-N21)*	*10.53 (10.40)*	*9.82*	LP(2)S25 → LP*(7)Zn29	0.80	21.61
LP(1)N26 → σ^*(C24-S25)	*46.09*	—	*LP(1)N22 → π^*(C24-S25)*	*34.87*	—	LP(1)S25 → LP*(8)Zn29	17.49	1.20
			LP(1)N22 → LP(1)C24*	*(58.01)*	*64.46 (64.40)*	LP(2)S25 → LP*(6)Zn29	69.54	50.55
			LP(2)S25 → LP*(6)Cu29	29.82	28.71	LP(2)S25 → LP*(8)Zn29	51.69	10.44
			LP(2)S25 → LP*(7)Cu29	20.94	24.77	LP(3)S25 → LP*(6)Zn29	4.59	66.42
			LP(3)S25 → LP(1)C24*	—	31.27	LP(3)S25 → LP*(7)Zn29	6.22	36.18
			LP(2)S25 → LP(1)C24*	—	10.05 (76.21)	*LP(2)S25 → σ^*(C24-N26)*	10.71	—
			LP(3)S25 → LP*(6)Cu29	—	26.22	*LP(2)S25 → LP*(1)C24*	—	38.26
			LP(3)S25 → LP*(7)Cu29	—	12.37	*LP(3)S25 → LP*(1)C24*	280.74	37.01
			LP(1)N26 → π^*(C24-S25)	*32.81*	—	*LP(1)N26 → LP*(1)C24*	*115.63*	*162.67*
			LP(1)N26 → LP(1)C24*	*(59.12)*	*84.10 (83.87)*			

[a]Refer to Figure 2 for atomic numbering.

[b]The $E^{(2)}$ values in parentheses are obtained from NBO data for the beta spin orbitals.

Table 9: Significant second-order interaction energies ($E^{(2)}$, kcal/mol) between donor and acceptor NBOs of the Ni(II), Pd(II), and Pt(II) chloride complexes of L1.

[Ni(L1)Cl_2]	$E^{(2)}$ (kcal/mol)		[Pd(L1)Cl_2]	$E^{(2)}$ (kcal/mol)		[Pt(L1)Cl_2]	$E^{(2)}$ (kcal/mol)	
Donor(i) → acceptor(j)	Gas-phase	DMSO	Donor(i) → acceptor(j)	Gas-phase	DMSO	Donor(i) → acceptor(j)	Gas-phase	DMSO
π(C6-C11) → π^*(C7-C8)	—	16.93	π(C6-C7) → π^*(C8-C9)	24.61	—	π(C6-C7) → π^*(C8-C9)	24.64	—
π(C6-C11) → π^*(C9-C10)	—	26.23	π(C6-C7) → π^*(C10-C11)	16.14	—	π(C6-C7) → π^*(C10-C11)	16.09	—
π(C7-C8) → π^*(C6-C11)	—	23.15	π(C6-C11) → π^*(C7-C8)	—	17.03	π(C7-C8) → LP*(*1*)C6	—	58.75
π(C7-C8) → π^*(C9-C10)	—	16.76	π(C6-C11) → π^*(C9-C10)	—	26.13	π(C7-C8) → π^*(C9-C10)	—	16.70
π(C7-C8) → LP*(1)C6	57.55	—	π(C7-C8) → π^*(C6-C11)	—	23.13	π(C8-C9) → π^*(C6-C7)	15.86	—
π(C7-C8) → LP(1)C9	42.41	—	π(C7-C8) → π^*(C9-C10)	—	16.91	π(C8-C9) → π^*(C10-C11)	21.01	—
π(C9-C10) → π^*(C6-C11)	—	17.00	π(C8-C9) → π^*(C6-C7)	15.92	—	π(C9-C10) → LP(1)C11	—	42.48
π(C9-C10) → π^*(C7-C8)	—	22.38	π(C8-C9) → π^*(C10-C11)	21.05	—	π(C9-C10) → π^*(C7-C8)	—	22.52
π(C9-C10) → π^*(C16-N21)	—	**10.57**	π(C9-C10) → π^*(C6-C11)	—	16.94	**π(C9-C10) → π^*(C16-N21)**	—	**10.31**
π(C10-C11) → LP*(1)C6	51.66	—	π(C9-C10) → π^*(C7-C8)	—	22.41	π(C10-C11) → π^*(C6-C7)	21.19	—
π(C10-C11) → LP(1)C9	42.27	—	π(C10-C11) → π^*(C6-C7)	21.16	—	π(C10-C11) → π^*(C8-C9)	17.03	—
σ(C16-N21) → LP*(5)Ni29	11.55	2.80	π(C10-C11) → π^*(C8-C9)	17.14	—	σ(C16-N21) → LP*(5)Pt29	10.59	11.15
σ(C16-N21) → LP*(7)Ni29	—	10.09	**π^*(C16-N21) → π^*(C8-C9)**	**39.26**	—	**π^*(C16-N21) → π^*(C8-C9)**	**33.48**	—
σ(S25-Ni29) → LP*(1)C24	11.77	0.80	**π^*(C16-N21) → π^*(C9-C10)**	—	**28.89**	**π^*(C16-N21) → π^*(C9-C10)**	—	**24.58**
σ^*(S25-Ni29) → LP*(5)Ni29	14.56	—	σ(S25-Pd29) → σ^*(C24-N26)	10.17	0.51	σ^*(S25-Pt29) → LP*(5)Pt29	36.64	38.36
σ^*(S25-Ni29) → LP*(6)Ni29	—	20.44	σ^*(S25-Pd29) → LP*(5)Pd29	26.54	219.1	LP(2)O2 → LP*(1)C6	—	59.60
LP(2)O2 → π^*(C6-C11)	—	29.43	σ^*(S25-Pd29) → LP*(6)Pd29	—	16.90	LP(2)O2 → π^*(C6-C7)	32.30	—
LP(2)O2 → LP*(1)C6	58.88	—	LP(2)O2 → π^*(C6-C7)	32.32	—	LP*(1)C6 → π^*(C7-C8)	—	55.77
LP(1)C9 → π^*(C7-C8)	75.01	—	LP(2)O2 → π^*(C6-C11)	—	29.38	LP(1)C11 → π^*(C9-C10)	—	88.87
LP(1)C9 → π^*(C10-C11)	64.80	—	LP(1)N21 → LP*(5)Pd29	57.82	69.97	LP(1)N21 → LP*(5)Pt29	89.27	95.65
LP(1)C9 → π^*(C16-N21)	**21.78**	—	LP(1)N21 → LP*(7)Pd29	—	40.41	LP(1)N21 → RY*(5)Pt29	6.41	14.74
LP(1)N21 → LP*(5)Ni29	89.26	56.13	LP(1)N21 → RY*(20)Pd29	1.66	10.41	LP(1)N21 → RY*(6)Pt29	14.99	12.30
LP(1)N21 → LP*(7)Ni29	—	62.68	*LP(1)N22 → π^*(C16-N21)*	*16.99*	*16.18*	LP(1)N21 → RY*(9)Pt29	12.77	8.23
LP(1)N22 → LP*(1)C24	*96.07*	*111.03*	*LP(1)N22 → LP*(1)C24*	—	*119.38*	LP(1)N21 → RY*(10)Pt29	18.13	17.98
LP(1)N22 → π^*(C16-N21)	*16.50*	*15.82*	*LP(1)N22 → π^*(C24-S25)*	*26.13*	—	LP(1)N21 → RY*(12)Pt29	14.82	16.96
LP(2)S25 → LP*(1)C24	*125.33*	*148.36*	LP(1)S25 → LP*(5)Pd29	—	13.31	LP(1)N21 → RY*(13)Pt29	18.11	18.46
LP(2)S25 → LP*(5)Ni29	3.27	12.32	LP(1)S25 → LP*(6)Pd29	—	18.47	LP(1)N21 → RY*(14)Pt29	12.53	17.21
LP(2)S25 → σ^*(S25-Ni29)	19.63	—	*LP(2)S25 → LP*(1)C24*	—	*139.93*	LP(1)N21 → RY*(16)Pt29	16.89	25.50
LP(1)N26 → LP*(1)C24	105.34	168.89	*LP(1)N26 → LP*(1)C24*	—	*169.32*	LP(1)*N21* → RY*(17)Pt29	2.90	21.51
LP*(1)C6 → π^*(C7-C8)	58.81	—	*LP(1)N26 → π^*(C24-S25)*	*34.62*	—	LP(1)N21 → RY*(18)Pt29	21.06	24.04
LP*(1)C6 → π^*(C10-C11)	55.05	—	LP(1)Pd29 → RY*(1)N21	12.36	—	LP(1)N21 → RY*(19)Pt29	23.29	1.35
LP*(5)Ni29 → RY*(1)N21	8.62	10.06	LP(2)Pd29 → RY*(1)N21	1.70	12.99	LP(1)N21 → RY*(20)Pt29	13.73	10.84
LP*(5)Ni29 → RY*(4)N21	8.91	11.29	LP(2)Pd29 → RY*(18)N21	—	10.73	*LP(1)N22 → π^*(C16-N21)*	16.01	15.64
LP*(5)Ni29 → RY*(6)N21	3.76	11.94	LP(2)Pd29 → RY*(20)N21	—	10.82	*LP(1)N22 → LP*(1)C24*	—	*115.02*
LP*(5)Ni29 → RY*(7)N21	1.84	11.76	LP*(5)Pd29 → RY*(1)N21	7.07	35.81	*LP(2)S25 → LP*(1)C24*	—	*138.8*
			LP*(5)Pd29 → RY*(2)N21	5.82	28.21	*LP(1)N22 → π^*(C24-S25)*	*43.67*	—
			LP*(5)Pd29 → RY*(3)N21	4.03	23.20	*LP(1)N26 → LP*(1)C24*	—	*168.64*
			LP*(5)Pd29 → RY*(5)N21	5.12	20.25	*LP(1)N2 → π^*(C24-S25)*	*52.15*	—
			LP*(5)Pd29 → RY*(6)N21	2.98	38.34	LP(1)Pt29 → RY*(1)N21	43.11	42.56
			LP*(5)Pd29 → RY*(7)N21	0.86	12.60	LP(1)Pt29 → RY*(2)N21	24.12	26.52
			LP*(5)Pd29 → RY*(9)N21	0.98	12.50	LP(1)Pt29 → RY*(5)N21	31.50	26.69

Table 9: Continued.

[Ni(L1)Cl_2]	$E^{(2)}$ (kcal/mol)		[Pd(L1)Cl_2]	$E^{(2)}$ (kcal/mol)		[Pt(L1)Cl_2]	$E^{(2)}$ (kcal/mol)	
Donor(i) → acceptor(j)	Gas-phase	DMSO	Donor(i) → acceptor(j)	Gas-phase	DMSO	Donor(i) → acceptor(j)	Gas-phase	DMSO
						LP(1)Pt29 → RY*(6)N21	22.21	27.81
						LP(1)Pt29 → RY*(1)N21	43.11	27.98
						LP(1)Pt29 → RY*(2)N21	24.12	23.92
						LP(1)Pt29 → RY*(5)N21	31.50	17.58
						LP(1)Pt29 → RY*(6)N21	22.21	18.69
						LP(5)Pt29 → RY*(1)N21	23.70	27.98

Refer to Figure 2 for atomic numbering.

complex is found to be extended from the benzene ring to the TSC moiety by the intensive hyperconjugative interactions π(C9-C10) $\rightarrow$ π^*(C16-N21), π^*(C16-N21) $\rightarrow$ π^*(C9-C10), π^*(C16-N21) $\rightarrow$ π^*(C8-C9), LP(1)N21 $\rightarrow$ σ^*(C9-C16), and LP(1)C9 $\rightarrow$ π^*(C16-N21). These are boldly highlighted in Tables 8 and 9.

Strong hyperconjugative interactions (italicized in Tables 8 and 9) predominate in the TSC moieties of all investigated molecules, giving rise to extensive electron delocalization that greatly improves the SHG efficiencies of the molecules. On the basis of their $E^{(2)}$ values, the strengths of the NBO interactions in all molecules studied are found to increase upon transition from the gas to the solvent phase. This partially accounts for the significant first hyperpolarizability increments of these molecules in the solvent environment. Strong donor-acceptor NBO interactions are found between the donor atoms (N21 and S25) of L1 and the transition metal ions in the MCl_2 fragments. The electrons donated by N21 and S25 are received in vacant metal-based lone pair (LP^*) and Rydberg (RY^*) orbitals. On the other hand, back donated electrons from the metal ions are mainly received in RY^* orbitals on N21. Back donation of electrons is highly significant in the Pd(II) and Pt(II) chloride complexes of L1 and minimal in the rest of the complexes, confirming the results earlier obtained from CDA analysis. Both CDA and NBO analyses have shown that the Pd(II) and Pt(II) ions can function as ambivalent electron donors and acceptors, while the Ni(II), Cu(II), and Zn(II) ions may only act as electron acceptors in their respective complexes investigated herein. It is also clear from NBO analysis that the π-conjugated pathways of these push-pull systems are comprised of the benzene ring and the attached TSC moieties.

4. Conclusion

Transition metal complexes containing π-conjugated organic ligands are less investigated for NLO applications despite their potentials of combining the high optical nonlinearity and chemical flexibility of organic materials with the physical strength of inorganic materials. Against this backdrop, the linked effects of transition metal chelation and solvent polarity on the first molecular hyperpolarizability (β_{tot}) of MAPTSC have been investigated herein via DFT calculations. Our results have revealed significant modifications of the β_{tot} value for MAPTSC upon complexation with different transition metal chlorides in the presence of solvents with varying dielectric constants. Therefore, its second-order NLO response is highly tunable by the synergy of transition metal chelation and solvent polarity. In gas-phase, the β_{tot} value for the thione tautomer of MAPTSC (L1) increases upon complexation with Pt(II) and Zn(II) chlorides, but decreases following its complexation with Ni(II), Pd(II), and Cu(II) chloride complexes. Nevertheless, the complexation of L1 with these transition metal chlorides in polar solvents results in modest to drastic first hyperpolarizability increments in nearly all cases studied. Based on these findings, it can be concluded that the complexation of a purely organic push-pull system with a transition metal center may not always improve upon its first hyperpolarizability vis-a-vis the NLO response, especially in the absence of a polar solvent. MAPTSC and its Zn(II) and Pt(II) chloride complexes have been identified as promising NLO materials because their gas-phase β_{tot} values are larger than those of the prototype push-pull molecules *para*-nitroaniline (PNA) and urea by factors of about 1.40–1.76 and 19.57–37.24, respectively; these factors greatly increase in polar solvent medium. Moreover, they have high optical transparencies in the visible region of the electromagnetic spectrum which greatly overcomes transparency/nonlinearity trade-offs that often lead to lower device efficiency and reduced photostability.

Competing Interests

The authors declare that there are no competing interests regarding the publication of this paper.

Acknowledgments

This work has been supported by a prospective joint research assistance sponsored by a CV Raman International Fellowship for African Researchers justifiable at IIT Kanpur, India (Grant no. 101F102), by the Ministry of External Affairs of India and FICCI (Federation of Indian Chambers of Commerce and Industry) for which the authors are grateful.

References

[1] T. Thilak, M. B. Ahamed, and G. Vinitha, "Third order nonlinear optical properties of potassium dichromate single crystals by Z-scan technique," *Optik*, vol. 124, no. 21, pp. 4716–4720, 2013.

[2] W.-Y. Wang, X.-F. Du, N.-N. Ma, S.-L. Sun, and Y.-Q. Qiu, "Theoretical investigation on switchable second-order nonlinear optical (NLO) properties of novel cyclopentadienylcobalt linear [4]phenylene complexes," *Journal of Molecular Modeling*, vol. 19, no. 4, pp. 1779–1787, 2013.

[3] C. Wang, C. Chen, Q. Zhang, D. Qi, and J. Jiang, "Nature of second-order nonlinear optical response in phthalocyanine derivatives: a density functional theory study," *Turkish Journal of Chemistry*, vol. 38, no. 6, pp. 1046–1055, 2014.

[4] A. Al-Yasari, N. Van Steerteghem, H. El Moll, K. Clays, and J. Fielden, "Donor-acceptor organo-imido polyoxometalates: high transparency, high activity redox-active NLO chromophores," *Dalton Transactions*, vol. 45, no. 7, pp. 2818–2822, 2016.

[5] R. Renjith, Y. S. Mary, C. Y. Panicker et al., "Spectroscopic (FT-IR, FT-Raman), first order hyperpolarizability, NBO analysis, HOMO and LUMO analysis of 1,7,8,9-tetrachloro-10,10-dimethoxy-4-[3-(4-phenylpiperazin-1-yl)propyl]-4-azatricyclo[5.2.1.$0^{2,6}$]dec-8-ene-3,5-dione by density functional methods," *Spectrochimica Acta Part A*, vol. 124, pp. 500–513, 2014.

[6] R. N. Singh and P. Rawat, "Spectral analysis, structural elucidation, and evaluation of both nonlinear optical properties and chemical reactivity of a newly synthesized ethyl-3,5-dimethyl-4-[(toluenesulfonyl)-hydrazonomethyl]-1H-pyrrole-2-carboxylate through experimental studies and quantum chemical calculations," *Journal of Molecular Structure*, vol. 1054-1055, pp. 65–75, 2013.

[7] J. Binoy, M. K. Marchewka, and V. S. Jayakumar, "The 'partial resonance' of the ring in the NLO crystal melaminium formate:

study using vibrational spectra, DFT, HOMO-LUMO and MESP mapping," *Spectrochimica Acta—Part A: Molecular and Biomolecular Spectroscopy*, vol. 104, pp. 97–109, 2013.

[8] Z. B. Liu, X. L. Zhang, X. Q. Yan, Y. S. Chen, and J. G. Tian, "Nonlinear optical properties of graphene-based materials," *Chinese Science Bulletin*, vol. 57, no. 23, pp. 2971–2982, 2012.

[9] K. S. Thanthiriwatte and K. M. Nalin de Silva, "Non-linear optical properties of novel fluorenyl derivatives—Ab initio quantum chemical calculations," *Journal of Molecular Structure: THEOCHEM*, vol. 617, pp. 169–175, 2002.

[10] P. Agarwal, N. Choudhary, A. Gupta, and P. Tandon, "Density functional theory studies on the structure, spectra (FT-IR, FT-Raman, and UV) and first order molecular hyperpolarizability of 2-hydroxy-3-methoxy-N-(2-chloro-benzyl)-benzaldehyde-imine: comparison to experimental data," *Vibrational Spectroscopy*, vol. 64, pp. 134–147, 2013.

[11] Z. Demircioğlu, Ç. A. Kaştaş, and O. Büyükgüngör, "The spectroscopic (FT-IR, UV-vis), Fukui function, NLO, NBO, NPA and tautomerism effect analysis of (E)-2-[(2-hydroxy-6-methoxybenzylidene)amino]benzonitrile," *Spectrochimica Acta Part A*, vol. 139, pp. 539–548, 2015.

[12] Y. Si, G. Yang, and Z. Su, "Chiroptical, linear, and second-order nonlinear optical properties of tetrathiafulvalenylallene: a multifunctional molecular material," *Journal of Materials Chemistry C*, vol. 1, no. 7, pp. 1399–1406, 2013.

[13] N. S. Labidi, "Nonlinear optical properties of novel mono-O-hydroxy bidentate schiff base: quantum chemical calculations," *International Journal of Metals*, vol. 2013, Article ID 964328, 5 pages, 2013.

[14] H. Alyar, "A review on nonlinear optical properties of donor-acceptor derivatives of naphthalene and azanaphthalene," *Reviews on Advanced Materials Science*, vol. 34, no. 1, pp. 79–87, 2013.

[15] F. Khammar, A. P. Kerasidou, K. Iliopoulos et al., "Effect of metal complexation on the nonlinear optical response of a conjugated ligand," *Journal of the Optical Society of America B: Optical Physics*, vol. 31, no. 7, pp. 1555–1560, 2014.

[16] S. A. Khan, A. M. Asiri, K. Al-Amry, and M. A. Malik, "Synthesis, characterization, electrochemical studies, and in vitro antibacterial activity of novel thiosemicarbazone and its Cu(II), Ni(II), and Co(II) complexes," *The Scientific World Journal*, vol. 2014, Article ID 592375, 9 pages, 2014.

[17] R. Santhakumari, K. Ramamurthi, G. Vasuki, B. M. Yamin, and G. Bhagavannarayana, "Synthesis and spectral characterization of acetophenone thiosemicarbazone—a nonlinear optical material," *Spectrochimica Acta Part A: Molecular and Biomolecular Spectroscopy*, vol. 76, no. 3-4, pp. 369–375, 2010.

[18] R. Kothari and B. Sharma, "Characterization, antibacterial, antifungal, antioxidant and DNA interaction studies of TSC transition metal complexes," *World Journal of Pharmacy and Pharmaceutical Sciences*, vol. 3, no. 7, pp. 1067–1080, 2014.

[19] E. G. Lewars, *Computational Chemistry: Introduction to the Theory and Applications of Molecular and Quantum Mechanics*, Springer, New York, NY, USA, 2nd edition, 2011.

[20] M. J. Frisch, G. W. Trucks, H. B. Schlegel et al., *Gaussian 09, Revision A.02*, Gaussian, Inc, Wallingford, Conn, USA, 2009.

[21] A. D. Becke, "Density-functional thermochemistry. III. The role of exact exchange," *The Journal of Chemical Physics*, vol. 98, no. 7, pp. 5648–5652, 1993.

[22] R. L. Martin, "Natural transition orbitals," *Journal of Chemical Physics*, vol. 118, no. 11, pp. 4775–4777, 2003.

[23] M. Karnan, V. Balachandran, M. Murugan, M. K. Murali, and A. Nataraj, "Vibrational (FT-IR and FT-Raman) spectra, NBO, HOMO-LUMO, Molecular electrostatic potential surface and computational analysis of 4-(trifluoromethyl)benzylbromide," *Spectrochimica Acta Part A*, vol. 116, pp. 84–95, 2013.

[24] H.-B. Liu, Y.-Q. Qiu, G.-C. Yang, C.-G. Liu, and S.-L. Sun, "Effects of electron donor and different solvents on polarizability and second hyperpolarizability of diradical complex involving X (X = B, Al, Ga)," *Chemical Research in Chinese Universities*, vol. 28, no. 2, pp. 308–312, 2012.

[25] A. Srivastava, R. Mishra, S. Kumar, K. Dev, P. Tandon, and R. Maurya, "Molecular structure, spectral investigation (^{1}H NMR, ^{13}C NMR, UV-Visible, FT-IR, FT-Raman), NBO, intramolecular hydrogen bonding, chemical reactivity and first hyperpolarizability analysis of formononetin [7-hydroxy-3(4-methoxyphenyl)chromone]: a quantum chemical study," *Journal of Molecular Structure*, vol. 1084, pp. 55–73, 2015.

[26] S. Ramalingam, M. Karabacak, S. Periandy, N. Puviarasan, and D. Tanuja, "Spectroscopic (infrared, Raman, UV and NMR) analysis, Gaussian hybrid computational investigation (MEP maps/HOMO and LUMO) on cyclohexanone oxime," *Spectrochimica Acta Part A*, vol. 96, pp. 207–220, 2012.

[27] J. G. Małecki, A. Maroń, M. Serda, and J. Polański, "Ruthenium(II) carbonyl complexes with thiosemicarbazone ligands," *Polyhedron*, vol. 56, pp. 44–54, 2013.

[28] R. Harness, C. Robertson, and F. Beckford, "Thiosemicarbazone complexes of group 12 elements. An investigation of the thiosemicarbazone from *p*-dimethylaminobenzaldehyde," *Journal of Undergraduate Chemistry Research*, vol. 7, no. 3, pp. 92–97, 2008.

[29] R. D. Dennington II, T. A. Keith, and J. M. Millam, *Gauss View 5.0.8*, Gaussian, Inc, Wallingford, Conn, USA, 2009.

[30] S. Dapprich and G. Frenking, "Investigation of donor-acceptor interactions: a charge decomposition analysis using fragment molecular orbitals," *Journal of Physical Chemistry*, vol. 99, no. 23, pp. 9352–9362, 1995.

[31] M. Xiao and T. Lu, "Generalized Charge Decomposition Analysis (GCDA) method," *Journal of Advances in Physical Chemistry*, vol. 4, no. 4, pp. 111–124, 2015.

[32] S. I. Gorelsky, S. Ghosh, and E. I. Solomon, "Mechanism of N_2O reduction by the μ_4-S tetranuclear Cu_Z cluster of nitrous oxide reductase," *Journal of the American Chemical Society*, vol. 128, no. 1, pp. 278–290, 2006.

[33] R. Z. Khaliullin, A. T. Bell, and M. Head-Gordon, "Analysis of charge transfer effects in molecular complexes based on absolutely localized molecular orbitals," *Journal of Chemical Physics*, vol. 128, no. 18, pp. 184112–184128, 2008.

[34] T. Lu and F. Chen, "Multiwfn: a multifunctional wavefunction analyzer," *Journal of Computational Chemistry*, vol. 33, no. 5, pp. 580–592, 2012.

[35] P. Song, C. Liu, W. Guan et al., "Theoretical investigation of second-order nonlinear optical response—Hexamolybdate as a superior donor over metal carbonyl complexes in the D-π-A model," *Canadian Journal of Chemistry*, vol. 89, no. 1, pp. 61–67, 2011.

[36] L. Jensen and P. T. van Duijnen, "The first hyperpolarizability of *p*-nitroaniline in 1,4-dioxane: a quantum mechanical/molecular mechanics study," *Journal of Chemical Physics*, vol. 123, no. 7, pp. 074307–074314, 2005.

[37] T. Sivaranjani, S. Xavier, and S. Periandy, "NMR, FT-IR, FT-Raman, UV spectroscopic, HOMO-LUMO and NBO analysis

of cumene by quantum computational methods," *Journal of Molecular Structure*, vol. 1083, pp. 39–47, 2015.

[38] S. Stoyanov, I. Petkov, L. Antonov, T. Stoyanova, P. Karagiannidis, and P. Aslanidis, "Thione-thiol tautomerism and stability of 2- and 4-mercaptopyridines and 2-mercaptopyrimidines," *Canadian Journal of Chemistry*, vol. 68, no. 9, pp. 1482–1489, 1990.

[39] X. Shan, A. O. Ibrahim, Y. Zhou et al., "Luminescent, second-order NLO and magnetic properties of the hydrogen-bond based network derived from 2,2′-bipyridine-6,6′-dicarboxylate," *Inorganic Chemistry Communications*, vol. 22, pp. 149–153, 2012.

[40] W. Humphrey, A. Dalke, and K. Schulten, "VMD: visual molecular dynamics," *Journal of Molecular Graphics*, vol. 14, no. 1, pp. 33–38, 1996.

[41] T. Lu and F. Chen, "Calculation of molecular orbital composition," *Acta Chimica Sinica*, vol. 69, no. 20, pp. 2393–2406, 2011.

[42] E. D. Glendening, A. E. Reed, J. E. Carpenter, and F. Weinhold, *NBO Version 3.1*, Gaussian Inc, Wallingford, Conn, USA, 2003.

[43] V. D. Vitnik, Ž. J. Vitnik, N. R. Banjac, N. V. Valentić, G. S. Ušćumlić, and I. O. Juranić, "Quantum mechanical and spectroscopic (FT-IR, 13C, 1H NMR and UV) investigations of potent antiepileptic drug 1-(4-chloro-phenyl)-3- phenyl-succinimide," *Spectrochimica Acta—Part A: Molecular and Biomolecular Spectroscopy*, vol. 117, pp. 42–53, 2014.